ADJOINT AND DEFECT ERROR BOUNDING AND CORRECTION FOR FUNCTIONAL ESTIMATES

NILES A. PIERCE* AND MICHAEL B. GILES†

*Applied & Computational Mathematics, California Institute of Technology

†Computing Laboratory, Oxford University

Two error estimation approaches are presented for the purposes of bounding or correcting the error in functional estimates such as lift or drag. Adjoint methods specifically quantify the error in a particular output functional due to residual errors in approximating the solution to the partial differential equation. Defect methods can used to bound or reduce the error in the entire solution, with corresponding improvements to functional estimates. The approaches may be used separately or in combination to obtain highly accurate solutions with asymptotically sharp error bounds. The adjoint theory is extended to handle flows with shocks and numerical experiments confirm 4th order error estimates for a pressure integral of shocked quasi-1D Euler flow. Numerical results also demonstrate 4th order accuracy for the drag on a cusped lifting airfoil at subsonic conditions.

Introduction

Integrals of solutions to partial differential equations (PDEs) provide crucial feedback on system behavior in many areas of engineering and science. In many settings, integral functional values are the primary quantitative outputs of numerical simulations to PDEs. In the field of computational fluid dynamics, lift and drag are computed as surface integrals of pressure and shear forces. The desire for efficient computational algorithms that produce reliable and accurate lift and drag values has motived a great deal of research during the last several decades. Integral functionals also arise in other aerospace areas such as the calculation of radar cross-sections in electromagnetics[1].

Modern numerical methods for PDEs make it possible to solve nonlinear systems with discontinuous solutions in complicated computational domains. Nonetheless, limited computational resources make it desirable to compute solutions to the minimum allowable accuracy. Supposing that the output of most interest is an integral functional, we arrive at two related challenges. For reliability, it is desirable to compute a bound on the remaining error in the functional. For efficiency, it is advantageous to compute the functional value to a higher order of accuracy than the overall solution on which it is based.

The present work describes two approaches to error bounding and error correction for functional estimates. Depending on the priorities of the engineer or scientist, an estimate of the leading term in the functional error may either be used to provide an asymptotically sharp error bound, or to remove the leading error term and obtain a superconvergent estimate. The first approach relies on the adjoint or dual PDE, whose solution describes the sensitivity of the functional of interest to residual errors in satisfying the original primal PDE . Smooth reconstructions of the primal and dual solutions are employed so the method is applicable equally to finite difference, finite volume or finite element discretizations[2–4]. The treatment of problems containing shocks requires careful consideration, and is addressed in this present work. A second approach uses the reconstructed primal solution to drive a defect iteration that improves the accuracy of the underlying baseline solution[4,5]. The resulting corrected solutions can be used to estimate the leading error term in the original functional estimate.

Adjoint sensitivities may also be employed as the basis for optimal adaptive meshing strategies[6,7] that seek to maximize the accuracy of the functional estimate for a given computational cost. The issues of error bounding and adaptive error control have received particular attention in the finite element community[1,8–21], where the use of the adjoint PDE for error analysis was first investigated. The orthogonality properties of most finite element methods ensure that functional estimates are naturally super-

*AIAA Member

†AIAA Member

AIAA Paper 2003-3846. 16th AIAA Computational Fluid Dynamics Conference, Orlando, FL, 2003.

convergent. The present approach may be used to enhance the natural finite element superconvergence [3] but it is also a generalization to other approximation methods.

The study of error convergence is particularly challenging if the true solution is unknown. To facilitate the study of functional accuracy for interesting physical systems and nontrivial computational domains, we formulate *modified* PDEs by postulating a solution and evaluating the source term that is required to make this the solution of the modified equations. If the postulated solution is close to a solution of the original PDE's, then the source term will be small and the modified problem will exercise the numerical method in a very similar manner to the true physics. In the present work, we describe modified Euler problems for two-dimensional flow in a duct, flow over a cylinder, and flow over a lifting Joukowski airfoil. These test cases have been invaluable for debugging error estimation algorithms.

Flows with shocks pose a major challenge to both adjoint calculations and adjoint error estimation. The correct formulation of the inviscid adjoint equations must account for linearised perturbations to the shock location. This approach reveals that the adjoint equations corresponding to the steady quasi-1D Euler equations require an interior boundary condition at the shock location [22]. Numerical results using either the "continuous" approach (approximating the analytical adjoint equations, using numerical smoothing in place of the shock boundary condition) or the "discrete" approach (linearising and transposing the discrete flow equations) yield convergent results[23].

Ulbrich has recently developed the analytical formulation of the adjoint equations for unsteady 1D equations with scalar fluxes, such as Burgers equation [24, 25]. In this case, numerical results [26] indicate that the "discrete" adjoint approach does not necessarily yield convergent results, unless one uses numerical dissipation that leads to an increasing smoothing of the shock as the mesh is refined. It seems likely that there will be similar problems with the convergence of solutions to the steady adjoint Euler equations in two dimensions, although such convergence errors may be very small for weak shocks.

In addition to these problems in calculating adjoint solutions, there is the further problem for adjoint error estimation that any smooth reconstructed solution must necessarily have an $O(1)$ local error near the shock so that the residual error is likely to increase without bound as the grid is refined. This undermines the whole basis for adjoint methods, which assume small errors, allowing a linearised treatment for error estimation. Here, we describe a new approach that circumvents these difficulties, by approximating the inviscid shock as the limiting structure of a viscous shock. Adjoint error estimates subsequently account for the error introduced by the nonzero viscosity and for the numerical error in approximating the viscous shock.

We begin by describing error bounding and correction alternatives using adjoint and defect methods. The approaches are then formulated for linear and nonlinear PDEs with inhomogeneous boundary conditions and bulk and boundary functionals. Additional theory is developed for the treatment of shocks and then numerical demonstrations are provided for smooth and shocked quasi-1D Euler flows, 2D duct flow, and flow over a lifting airfoil.

Error Bounding and Correction

Adjoint and defect methods based on smooth solution reconstructions are employed to bound and correct errors in estimates of integrals functionals. The basic methods and alternatives are now introduced in the simplest scenario of a linear differential equation with homogeneous boundary conditions and a bulk functional.

Adjoint Methods

Consider the linear differential equation

$$Lu = f$$

subject to homogeneous boundary conditions on the domain Ω. Suppose we are interested in evaluating the linear functional (g, u), where $(.,.)$ denotes an integral inner product on Ω. This functional may equivalently be evaluated in the dual form (v, f), where v is the solution to the dual or adjoint PDE

$$L^* v = g,$$

subject to homogeneous adjoint boundary conditions. The equivalence of the primal and dual functional representations follows from the definition of the adjoint operator

$$(v, f) = (v, Lu) \equiv (L^* v, u) = (g, u).$$

The dual form of the functional indicates that the adjoint solution v represents the sensitivity of the functional to the primal source term f.

Discrete approximate primal and dual solutions, U_h and V_h, are computed on a mesh of average interval h. Smooth reconstructions are then obtained

$$u_h \equiv R_h U_h, \quad v_h \equiv R_h V_h,$$

where R_h is a reconstruction operator (e.g. linear or cubic spline interpolation). The degree to which these functions do not satisfy the original PDEs can then be quantified by the primal and dual *residual errors* defined by

$$Lu_h - f = L(u_h - u), \quad L^* v_h - g = L^*(v_h - v).$$

Assuming that the underlying physical solution is sufficiently smooth, the anticipated order of convergence for the functional estimate depends on:

n, the order of the operator L,

p, the order of the discrete solution,

r, the order of the reconstruction.

Intuitively, the solution and residual errors are expected to satisfy

$$\begin{aligned} \|u_h - u\|, \ \|v_h - v\| &= O\left(h^{\min(p,r)}\right) \qquad (1) \\ \|Lu_h - f\|, \ \|L^* v_h - g\| &= O\left(h^{\min(p,r-n)}\right), \end{aligned}$$

where the n differentiations required to evaluate the residual errors account for their reduced accuracy. In practice, these results may only hold in certain norms.

The error in the functional value based on the reconstructed primal solution may be expressed as

$$\begin{aligned} (g,u) - (g,u_h) &= (g, u - u_h) \\ &= (L^* v, u - u_h) \\ &= (v, L(u - u_h)) \\ &= (v, f - Lu_h). \end{aligned}$$

Introducing the reconstructed adjoint solution v_h gives

$$(g,u) - (g,u_h) = (v_h, f - Lu_h) + (v - v_h, f - Lu_h).$$

The first term on the right hand side can be evaluated, since f, u_h and v_h are all known. The second term cannot be evaluated because v is not known, however from 1 it can be a factor $O(h^{\min pr})$ smaller than the first. Therefore we can use the first term as an error bound,

$$|(g,u) - (g,u_h)| \leq |(v_h, f - Lu_h)| \qquad (2)$$

which is sharp asymptotically as h decreases, but may be violated for finite h. Multiplying the error bound by any constant greater than unity will ensure that it is a valid bound for sufficiently small h, but it is not possible in general to say how small h must be.

Alternatively, the first term can be moved to the left hand side to obtain a more accurate functional estimate

$$(g,u) - \Big\{(g,u_h) + (v_h, f - Lu_h)\Big\} = (v - v_h, f - Lu_h). \qquad (3)$$

As a concrete example, consider a one-dimensional Poisson problem

$$L = L^* = \frac{\mathrm{d}^2}{\mathrm{d}x^2}, \quad f = x^3(1-x)^3, \quad g = \sin \pi x$$

with homogeneous boundary conditions on $x \in [0,1]$. The problem is discretized using second order finite differences and solution reconstruction is performed using cubic spline interpolation ($n = 2$, $p = 2$, $r = 4$). Integrals are evaluated using 3-point Gauss quadrature.

¿From estimates (1), the reconstructed primal and dual solutions are $O(h^2)$. Also, the functional estimate (g, u_h) has the same order of accuracy as the primal solution on which it is based. The remainder term in (2) and (3) is of order

$$\begin{aligned} |(v - v_h, f - Lu_h)| &= O\left(h^{\min(2,4)+\min(2,4-2)}\right) \\ &= O(h^4). \end{aligned}$$

Using adjoint error bounding, we expect a 2nd order functional estimate with an asymptotically sharp error bound that itself contains a 4th order error. Alternatively, using adjoint error correction, we expect a 4th order functional estimate. These two alternatives are illustrated by the numerical results in Figure 1a. Lines of slope -2 and -4 are drawn through the error value on the finest mesh to assist in determining the convergence rate. Note that the error bound is indistinguishable from the remaining error, as it is roughly 10^2 times more accurate than the functional estimate on the coarsest mesh, increasing to roughly 10^5 times more accurate on the finest mesh. Using adjoint error correction, rigorous *a priori* analysis of the errors in the primal and dual numerical solutions as well as the errors associated with the spline reconstruction confirms that the functional accuracy should in fact double in accuracy from 2nd to 4th order[27].

Depending on the reconstruction method, it is possible that the inner product $(v - v_h, f - Lu_h)$ or equivalently $(g - L^* v_h, u - u_h)$ will exhibit a convergence rate that is *faster* than the product of the convergence rates of its components. This results from cancellation effects that have been observed and analyzed in the nonlinear case of smooth quasi-1D Euler flow[27].

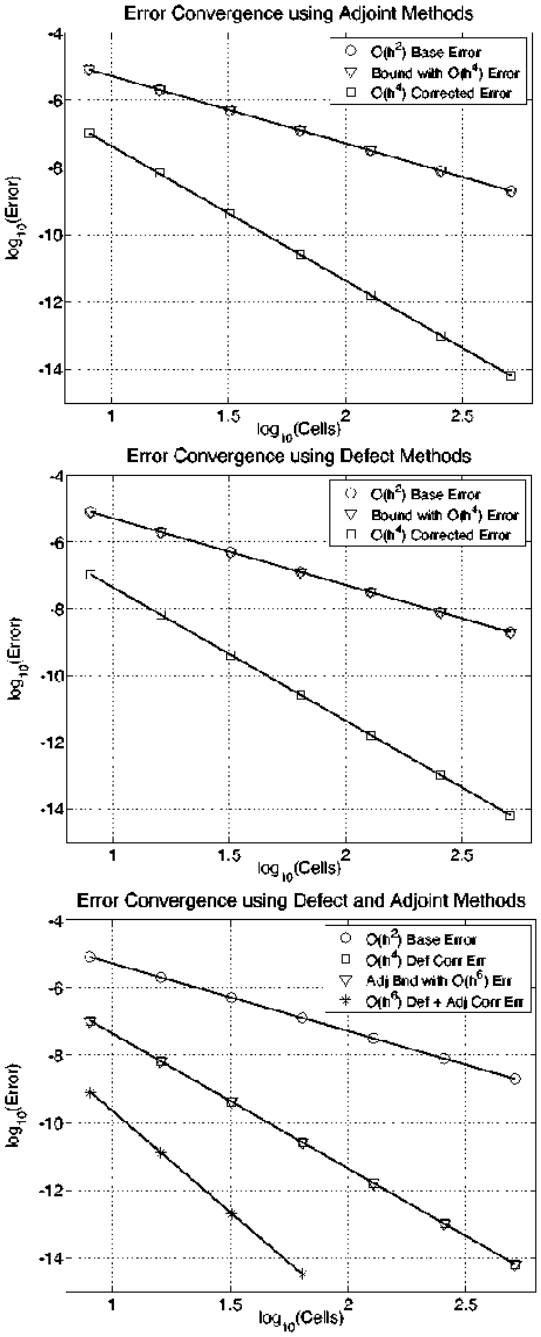

Figure 1. Functional estimates for a 1D Poisson problem: a) Adjoint error bounding and correction, b) Defect error bounding and correction, c) Defect error correction followed by adjoint error bounding or correction. The superimposed lines have slopes of -2,-4 or -6 as suggested by the rate descriptions in the legends.

Defect Methods

As an alternative to adjoint methods, solution reconstruction may be used to drive a defect correction process. If the original numerical solution is obtained by solving the discrete problem

$$L_h U_h = T_h f$$

where T_h is an operator that transfers the continuous source term f to discrete source terms associated with the each of the unknowns in U_h, then the defect correction iteration may be written as

$$\begin{aligned} L_h \Delta U_h &= T_h \left(f - L u_h\right) \\ u_{dh} &= u_h + R_h \Delta U_h, \end{aligned} \tag{4}$$

where R_h is the linear reconstruction operator[4,5]. Note that this defect correction procedure differs from traditional defect correction approaches that evaluate Lu_h using a higher order discrete operator L'_h applied to the low order solution U_h (instead of the differential operator L applied to the reconstructed solution u_h).

If the defect iteration is convergent, the final accuracy of the defect corrected approximate solution u_{dh} is determined *not* by the low order discrete operator L_h used to obtain the solution, but instead by the interpolation accuracy of the reconstruction method used to form u_h and u_{dh}.

Using the reconstructed defect solution u_{dh}, the error in the original functional estimate may be represented

$$(g,u) - (g,u_h) = (g, u_{dh} - u_h) + (g, u - u_{dh})$$

where the first term on the right hand side may be evaluated to provide an asymptotically sharp error bound

$$|(g,u) - (g,u_h)| \leq |(g, u_{dh} - u_h)|$$

or subtracted to give a more accurate functional estimate

$$(g,u) - (g,u_h) - (g, u_{dh} - u_h) = (g, u - u_{dh}). \tag{5}$$

For the previously considered 1D Poisson problem, defect correction of the primal solution using cubic spline reconstruction yields 4th order solution errors and consequently a 4th order functional estimate. The behavior for error bounding and correction is illustrated in Figure 1b.

Combined Adjoint and Defect Methods

Combined approaches yield even sharper error estimates. The remaining error in (5) may be expressed in the dual form

$$\begin{aligned} (g,u) - (g,u_h) - (g, u_{dh} - u_h) &= (g, u - u_{dh}) \\ &= (L^* v, u - u_{dh}) \\ &= (v, L(u - u_{dh})) \\ &= (v, f - L u_{dh}). \end{aligned}$$

We introduce the reconstructed dual solution v_h

$$(g,u) - (g,u_h) - (g,u_{dh}-u_h) \\ = (v_h, f-Lu_{dh}) + (v-v_h, f-Lu_{dh}).$$

and evaluate the first term on the right hand side to obtain either the asymptotically sharp error bound

$$|(g,u) - (g,u_h) - (g,u_{dh}-u_h)| \leq |(v_h, f-Lu_{dh})|$$

or the more accurate functional estimate

$$\begin{aligned}(g,u) - (g,u_h) - (g,u_{dh}-u_h) - (v_h, f-Lu_{dh}) & \\ = (v-v_h, f-Lu_{dh}) & \\ = (g-L^*v_h, u-u_{dh}). & \quad (6)\end{aligned}$$

For the 1D Poisson problem, the order of the remainder term may be estimated as

$$\begin{aligned}(g-L^*v_h, u-u_{dh}) &= O\left(h^{\min(2,4-2)+\min(4,4)}\right) \\ &= O(h^6).\end{aligned}$$

Note that an estimate based on the alternative dual representation of the remainder in (6) would appear to be only $O(h^4)$. Integration by parts to obtain the primal form shows that this estimate is overly pessimistic. Hence, in the numerical results of Figure 1c, we observe either a 4th order functional estimate with a sharp error bound that itself contains a 6th order error, or else a 6th order functional estimate without a computable bound.

Linear Formulation

Adjoint Error Estimates

We now extend the adjoint error estimation approach to problems with inhomogeneous boundary conditions and output functionals that contain boundary integrals[2,4].

Let u be the solution of the linear differential equation

$$Lu = f,$$

in the domain Ω, subject to the linear boundary conditions

$$Bu = e,$$

on the boundary $\partial\Omega$. In general, the number of boundary conditions described by the operator B may be different on different parts of the boundary (e.g. inflow and outflow sections for hyperbolic problems).

The output functional of interest is taken to be

$$J = (g,u) + (h, Cu)_{\partial\Omega},$$

where $(.,.)_{\partial\Omega}$ represents an integral inner product over the boundary $\partial\Omega$. The boundary operator C may be algebraic (e.g. $Cu \equiv u$) or differential (e.g. $Cu \equiv \frac{\partial u}{\partial n}$). As with the boundary condition operator B, the boundary functional operator C may have different numbers of components on different parts of the boundary. The corresponding components of h may be set to zero on those parts of the boundary where the functional does not have a boundary integral contribution.

The corresponding linear adjoint problem is

$$L^*v = g,$$

in Ω, subject to the boundary conditions

$$B^*v = h,$$

on the boundary $\partial\Omega$. The fundamental identity defining L^*, B^* and the boundary operator C^* is

$$(v, Lu) + (C^*v, Bu)_{\partial\Omega} = (L^*v, u) + (B^*v, Cu)_{\partial\Omega},$$

for all u, v. This identity is obtained by integration by parts and it implies that the primal functional operator C and the adjoint boundary condition operator B^* contain an equal number of components at any location on the boundary. The construction of the appropriate adjoint operators for the linearised Euler and Navier-Stokes equations is described elsewhere[28-30].

Using the adjoint identity, the equivalent dual form of the output functional is

$$J = (v,f) + (C^*v, e)_{\partial\Omega}.$$

Given approximate reconstructed solutions u_h and v_h, the error in the functional may be expressed

$$\begin{aligned}&(g,u) + (h,Cu)_{\partial\Omega} - (g,u_h) - (h,Cu_h)_{\partial\Omega} \\ &= -(L^*v_h, u_h-u) - (B^*v_h, C(u_h-u))_{\partial\Omega} \\ &\quad +(L^*v_h-g, u_h-u) + (B^*v_h-h, C(u_h-u))_{\partial\Omega} \\ &= -(v_h, L(u_h-u)) - (C^*v_h, B(u_h-u))_{\partial\Omega} \\ &\quad +(L^*(v_h-v), u_h-u) + (B^*(v_h-v), C(u_h-u))_{\partial\Omega} \\ &= -(v_h, Lu_h-f) - (C^*v_h, Bu_h-e)_{\partial\Omega} \\ &\quad +(v_h-v, L(u_h-u)) + (C^*(v_h-v), B(u_h-u))_{\partial\Omega}.\end{aligned}$$

In the final result, the first line comprises computable adjoint error estimates that describe the influence of the bulk and boundary residuals on the functional of interest. These terms may either be used to obtain a more accurate solution or to provide an asymptotically sharp bound on the error in the original functional estimate. The second line describes the higher order remaining error.

Defect Error Estimates

The linear defect iteration (4) can be generalized to inhomogeneous boundary conditions by ensuring that the reconstruction satisfies the analytical boundary conditions at the discrete mesh points located on the boundary.

Nonlinear Formulation

This section describes the extension of the linear theory to nonlinear operators and functionals[2,4]. It begins with some definitions and observations regarding the linearization of functions and operators.

Preliminaries

If u is a scalar variable and $f(u)$ is a nonlinear scalar function then a standard Taylor series expansion gives

$$f(u_2) = f(u_1) + f'(u_1)\ (u_2-u_1) + O((u_2-u_1)^2).$$

Alternatively, an exact expression without remainder terms is obtained by starting from

$$\frac{d}{d\theta} f\left(u_1+\theta(u_2-u_1)\right) = f'\left(u_1+\theta(u_2-u_1)\right)\ (u_2-u_1),$$

and then integrating from $\theta=0$ to $\theta=1$ to give

$$f(u_2) - f(u_1) = \overline{f'}_{(u_1,u_2)}\ (u_2 - u_1),$$

where

$$\overline{f'}_{(u_1,u_2)} \equiv \int_0^1 f'\left(u_1+\theta(u_2-u_1)\right)\ \mathrm{d}\theta.$$

For the nonlinear operator $N(u)$, the corresponding linearised operator L_u is defined formally by the Fréchet derivative

$$L_u\tilde{u} \equiv \lim_{\varepsilon\to 0} \frac{N(u+\varepsilon\tilde{u}) - N(u)}{\varepsilon}.$$

The subscript u denotes that L_u depends on the value of u around which $N(u)$ is linearized. For example, if

$$N(u) = \frac{\partial}{\partial x}\left(\tfrac{1}{2}u^2\right) - \nu\,\frac{\partial^2 u}{\partial x^2}$$

then

$$L_u\tilde{u} = \frac{\partial}{\partial x}\left(u\,\tilde{u}\right) - \nu\,\frac{\partial^2 \tilde{u}}{\partial x^2}.$$

Starting from

$$\frac{d}{d\theta}\ N\left(u_1+\theta(u_2-u_1)\right) = L_{u_1+\theta(u_2-u_1)}\ (u_2-u_1)$$

and integrating over θ

$$N(u_2) - N(u_1) = \overline{L}_{(u_1,u_2)}\ (u_2-u_1),$$

where

$$\overline{L}_{(u_1,u_2)} = \int_0^1 L|_{u_1+\theta(u_2-u_1)}\ \mathrm{d}\theta.$$

Thus $\overline{L}_{(u_1,u_2)}$ is the average linear operator over the "path" from u_1 to u_2.

Adjoint Error Estimates

Let u be the solution of the nonlinear differential equation

$$N(u) = 0$$

in the domain Ω, subject to the nonlinear boundary conditions

$$D(u) = 0$$

on the boundary $\partial\Omega$.

The linear differential operators L_u and B_u are defined by the Fréchet derivatives of N and D, respectively,

$$L_u\,\tilde{u} \equiv \lim_{\epsilon\to 0} \frac{N(u+\epsilon\tilde{u}) - N(u)}{\epsilon},$$

$$B_u\,\tilde{u} \equiv \lim_{\epsilon\to 0} \frac{D(u+\epsilon\tilde{u}) - D(u)}{\epsilon}.$$

It is assumed that the nonlinear functional of interest, $J(u)$, has a Fréchet derivative of the following form,

$$\lim_{\epsilon\to 0} \frac{J(u+\epsilon\tilde{u}) - J(u)}{\epsilon} = (g(u),\tilde{u}) + (h, C_u\tilde{u})_{\partial\Omega}.$$

where the operator C_u may be algebraic or differential.

The corresponding linear adjoint problem is

$$L_u^* v = g(u)$$

in Ω, subject to the boundary conditions

$$B_u^* v = h$$

on the boundary $\partial\Omega$. The adjoint identity defining L_u^*, B_u^* and the boundary operator C_u^* is

$$(v, L_u\tilde{u}) + (C_u^* v, B_u\tilde{u})_{\partial\Omega} = (L_u^* v, \tilde{u}) + (B_u^* v, C_u\tilde{u})_{\partial\Omega},$$

for all $\tilde{u}, v$. This expression implies that B_u^* has the same number of components as $C(u)$ at any point on the boundary.

We now consider approximate reconstructed primal and dual solutions u_h and v_h. The error analysis that follows makes use of the quantities

$$L^*_{u_h} v_h, \quad B^*_{u_h} v_h, \quad C^*_{u_h} v_h,$$

which are computable since the linear operators are defined based on u_h rather than u. The analysis also requires averaged Fréchet derivatives defined by

$$\begin{aligned}
\overline{L}_{(u,u_h)} &= \int_0^1 L|_{u+\theta(u_h-u)}\, d\theta, \\
\overline{B}_{(u,u_h)} &= \int_0^1 B|_{u+\theta(u_h-u)}\, d\theta, \\
\overline{C}_{(u,u_h)} &= \int_0^1 C|_{u+\theta(u_h-u)}\, d\theta, \\
\overline{g}(u,u_h) &= \int_0^1 g(u+\theta(u_h-u))\, d\theta,
\end{aligned}$$

so that

$$\begin{aligned}
N(u_h)-N(u) &= \overline{L}_{(u,u_h)}\,(u_h-u), \\
D(u_h)-D(u) &= \overline{B}_{(u,u_h)}\,(u_h-u), \\
J(u_h)-J(u) &= (\overline{g}(u,u_h), u_h-u) \\
&+ (h, \overline{C}_{(u,u_h)}(u_h-u))_{\partial\Omega}.
\end{aligned}$$

Adjoint error estimates may then be expressed

$$\begin{aligned}
& J(u_h) - J(u) \\
&= (\overline{g}(u,u_h), u_h-u) + (h, \overline{C}_{(u,u_h)}(u_h-u))_{\partial\Omega} \\
&= (L^*_{u_h} v_h, u_h-u) + (B^*_{u_h} v_h, C_{u_h}(u_h-u))_{\partial\Omega} \\
&\quad -(L^*_{u_h} v_h - \overline{g}(u,u_h), u_h-u) \\
&\quad -(h, (C_{u_h} - \overline{C}_{(u,u_h)})(u_h-u))_{\partial\Omega} \\
&\quad -(B^*_{u_h} v_h - h, C_{u_h}(u_h-u))_{\partial\Omega} \\
&= (v_h, L_{u_h}(u_h-u)) + (C^*_{u_h} v_h, B_{u_h}(u_h-u))_{\partial\Omega} \\
&\quad -(L^*_{u_h} v_h - \overline{g}(u,u_h), u_h-u) \\
&\quad -(h, (C_{u_h} - \overline{C}_{(u,u_h)})(u_h-u))_{\partial\Omega} \\
&\quad -(B^*_{u_h} v_h - h, C_{u_h}(u_h-u))_{\partial\Omega} \\
&= (v_h, \overline{L}_{(u,u_h)}(u_h-u)) + (C^*_{u_h} v_h, \overline{B}_{(u,u_h)}(u_h-u))_{\partial\Omega} \\
&\quad -(L^*_{u_h} v_h - \overline{g}(u,u_h), u_h-u) \\
&\quad -(h, (C_{u_h} - \overline{C}_{(u,u_h)})(u_h-u))_{\partial\Omega} \\
&\quad -(B^*_{u_h} v_h - h, C_{u_h}(u_h-u))_{\partial\Omega} \\
&\quad +(v_h, (L_{u_h} - \overline{L}_{(u,u_h)})(u_h-u)) \\
&\quad +(C^*_{u_h} v_h, (B_{u_h} - \overline{B}_{(u,u_h)})(u_h-u))_{\partial\Omega} \\
&= (v_h, N(u_h)) + (C^*_{u_h} v_h, D(u_h))_{\partial\Omega} \\
&\quad -(L^*_{u_h} v_h - \overline{g}(u,u_h), u_h-u) \\
&\quad -(h, (C_{u_h} - \overline{C}_{(u,u_h)})(u_h-u))_{\partial\Omega} \\
&\quad -(B^*_{u_h} v_h - h, C_{u_h}(u_h-u))_{\partial\Omega} \\
&\quad +(v_h, (L_{u_h} - \overline{L}_{(u,u_h)})(u_h-u)) \\
&\quad +(C^*_{u_h} v_h, (B_{u_h} - \overline{B}_{(u,u_h)})(u_h-u))_{\partial\Omega}.
\end{aligned}$$

In the final result, the first line contains adjoint error estimation terms describing the influence of the residual errors in satisfying the PDE and the boundary conditions. These terms may be used either to provide an asymptotically sharp bound on the error in the functional estimate or to correct the error to leading order. The other lines are the remaining errors, which include the consequences of nonlinearity in L, B, C and g as well as residual errors in approximating the adjoint problem.

If the solution errors for the nonlinear primal problem and the linear adjoint problem are of the same order, and they are both sufficiently smooth that the corresponding residual errors are also of the same order, then the order of accuracy of the functional approximation after making the adjoint correction is twice the order of the primal and adjoint solutions. However, rigorous *a priori* and *a posteriori* analysis of the remaining errors is much harder than in the linear case[27].

Defect Error Estimates

Suppose the original nonlinear PDE has the discretization

$$N_h(U_h) = 0$$

including appropriate boundary conditions. The defect calculation has the appearance of an approximate Newton iteration

$$\begin{aligned}
\frac{\partial N_h}{\partial U_h}\,\Delta U_h &= -T_h N(u_h), \\
u_{dh} &= u_h + R_h \Delta U_h,
\end{aligned}$$

where it is important to note that the right hand side is based on the differential operator N acting on the reconstructed solution u_h. The analytical boundary conditions are imposed on u_h at the mesh points on the boundary prior to using the reconstructed solution to drive the defect process.

If a linearized discretization has not been previously implemented, it may be more convenient to base the defect iteration on the nonlinear discretization, replacing the first step by

$$N_h(U_h+\Delta U_h) - N_h(U_h) = -T_h N(u_h),$$

which simplifies to

$$N_h(U_h+\Delta U_h) = -T_h N(u_h).$$

Adjoint Approach for Shocked Flows

Non-oscillatory shock-capturing schemes have revolutionized the calculation of transonic flows, providing one-point shock structures. Unfortunately, sharp shocks introduce fundamental difficulties when attempting to use linearization approaches to evaluate the sensitivities of functionals to solution errors. In fact, a convergent nonlinear discretization may have linear sensitivities that do not converge[26].

One solution to this problem is to approach it from the perspective of well-resolved viscous shocks. Let u_ε be the solution of the "viscous" quasi-1D Euler equations

$$\frac{\partial}{\partial x}\begin{pmatrix} A\rho q_x \\ A\rho q_x^2 \\ A\rho q_x H \end{pmatrix} + A\,\frac{\partial}{\partial x}\begin{pmatrix} 0 \\ p \\ 0 \end{pmatrix} = A\varepsilon\,\frac{\partial^2}{\partial x^2}\begin{pmatrix} \rho \\ q_x \\ p \end{pmatrix},$$

where $A(x)$ is the duct area. This may be written symbolically as

$$N(u_\varepsilon) = \varepsilon\, S(u_\varepsilon). \tag{7}$$

In the limit $\varepsilon \to 0$, u_ε will converge to the discontinuous inviscid solution u at every point except at the shock point. If $u_{\varepsilon,h}$ is an approximation to u_ε, then the error in the computed value of the functional $J(u)$ may be split into two parts

$$\begin{aligned} J(u) - J(u_{\varepsilon,h}) &= \big(J(u) - J(u_\varepsilon)\big) \\ &+ \big(J(u_\varepsilon) - J(u_{\varepsilon,h})\big). \end{aligned}$$

The first part is the error due to the viscosity. A matched inner and outer asymptotic analysis[31,32] reveals that for functionals such as the integrated pressure,

$$J(u_\varepsilon) = J(u) + a\,\varepsilon + O(\varepsilon^2),$$

for some constant a. Accordingly,

$$J(u) - J(u_\varepsilon) = -\varepsilon\,\frac{\mathrm{d}}{\mathrm{d}\varepsilon}J(u_\varepsilon) + O(\varepsilon^2),$$

where the quantity

$$\frac{\mathrm{d}}{\mathrm{d}\varepsilon}J(u_\varepsilon) = \left(g(u_\varepsilon), \frac{\mathrm{d}u_\varepsilon}{\mathrm{d}\varepsilon}\right)$$

may be evaluated by the adjoint approach since by definition, the gradient with respect to ε is based on infinitesimal perturbations to the viscous solution. Differentiating (7) with respect to ϵ gives

$$L_{u_\varepsilon}\frac{\mathrm{d}u_\varepsilon}{\mathrm{d}\varepsilon} = S(u_\varepsilon),$$

where L_{u_ε} is the Fréchet derivative of the nonlinear operator $N-\varepsilon S$. Hence,

$$\left(g(u_\varepsilon), \frac{\mathrm{d}u_\varepsilon}{\mathrm{d}\varepsilon}\right) = (v_\varepsilon, S(u_\varepsilon)),$$

assuming that the viscous adjoint solution v_ε exactly satisfies the inviscid boundary conditions. If $v_{\varepsilon,h}$ is an approximation to the viscous adjoint v_ε, then $\varepsilon(v_{\varepsilon,h}, S(u_{\varepsilon,h}))$ is an approximation to the functional error due to the viscosity.

The second part of the error in (8) is due to the approximation of the solution to the viscous equation. With a well-resolved shock, it is possible to ensure that $u_\varepsilon - u_{\varepsilon,h}$ is small, so the resulting functional error can be approximated by usual adjoint estimate $(v_{\varepsilon,h}, N(u_{\varepsilon,h}) - \varepsilon S(u_{\varepsilon,h}))$. Adding this second term to the first term due to the viscosity gives the combined adjoint error estimate

$$\begin{aligned} \big(v_{\varepsilon,h},\ N(u_{\varepsilon,h}) - \varepsilon S(u_{\varepsilon,h})\big) + \varepsilon\,\big(v_{\varepsilon,h},\ S(u_{\varepsilon,h})\big) \\ = \big(v_{\varepsilon,h},\ N(u_{\varepsilon,h})\big) \end{aligned}$$

It is quite striking that the final result simplifies to the standard adjoint error approximation using the *inviscid* operator N but the "viscous" approximate solutions $u_{\varepsilon,h}$ and $v_{\varepsilon,h}$. Since the viscous operator is not applied to the reconstructed solutions, the treatment of shocked flows imposes no additional accuracy requirements on the reconstruction scheme.

We conjecture that a similar treatment may be used for contact discontinuities. In that setting, the smoothing introduced by viscosity ε leads to a functional error which is $O(\sqrt{\varepsilon})$ to leading order. Hence, the final form of the adjoint correction will not have quite such a pleasingly simple form.

One-dimensional Results

The error estimation capabilities of adjoint and defect methods are now demonstrated for a sequence of nonlinear problems.

Subsonic quasi-1D duct

We first consider subsonic quasi-1D Euler flow in a converging-diverging nozzle

$$A(x) = \begin{cases} 2, & -1 \le x \le -\frac{1}{2}, \\ 2 - \sin^4[\pi(x+\frac{1}{2})], & -\frac{1}{2} < x < \frac{1}{2}, \\ 2, & \frac{1}{2} \le x \le 1, \end{cases} \tag{8}$$

with a functional that is the integral of pressure. The flow is fully determined by specifying stagnation enthalpy ($H = 4$) and stagnation pressure ($p_0 = 2$) at

the inlet and pressure ($p = 1.9$) at the exit. The numerical solution of Figure 2a is computed using a second order finite volume scheme and reconstructed using cubic spline interpolation. Integrals are evaluated using 3-point Gauss quadrature so that the numerical integration errors are $O(h^6)$ [33]. The exact geometry is employed when evaluating the flow residual.

The performance of adjoint error bounding and correction is illustrated in Figure 2b. The bound is sharp, containing an $O(h^4)$ error compared to the $O(h^2)$ accuracy of the functional estimate. By subtracting the leading error term, we obtain an $O(h^4)$ functional estimate. Note that the temporary excursion of the base error from the overall trend is caused by a change in the sign of the error.

It is surprising that very similar error estimates are obtained using piecewise linear reconstruction. Linear interpolation provides $O(h^2)$ solution accuracy but only $O(h)$ residuals (as a result of differentiating once). Hence, the corrected functional estimate is expected to be only $O(h^3)$. However, numerical experiments reveal that the functional accuracy is actually $O(h^4)$, as seen in Figure 2c. This unexpected accuracy results from a cancellation effect between the leading order terms in the adjoint solution and the flow residual that has been elucidated for the quasi-1D Euler equations[27].

Returning to cubic spline reconstruction, the combined use of defect and adjoint error correction is illustrated in Figure 2d. The 2nd order base error is bounded by the defect error estimate, or alternatively, it is corrected to obtain 4th order accuracy. Adjoint methods are then used to obtain a sharp bound on the 4th order functional estimate or alternatively, a 7th order functional estimate is obtained by subtracting the adjoint correction. The primal solution is $O(h^4)$ and the adjoint residual is $O(h^2)$ so we expect $O(h^6)$ accuracy. The higher observed rate of convergence may be related to the choice of geometry or it may result from a cancellation effect. The 7th order accuracy is also observed for a related asymmetrical geometry.

Shocked quasi-1D duct

We now consider the integral of pressure for shocked flow in an expanding duct. The geometry is defined by the quintic polynomial $A(x)$ that yields $A'(x) = A''(x) = 0$ at $x = 0, 1$ with $A(0) = 0.95$ and $A(1) = 1.05$. Uniform inlet and outlet sections of length 0.1 are appended to this smooth expansion. The flow and adjoint solutions are both obtained using second order finite volume schemes. Hence, the errors in the functional resulting from viscosity and from the discretization error are both second order.

Adjoint error correction is implemented using two adaptive meshing approaches: grid redistribution and grid refinement. Using grid redistribution, grid points are moved to better resolve regions with high gradients and/or second derivatives. Using grid refinement, extra grid points are added by subdividing cells to better resolve the gradients in the shock region. In this implementation, both methods used a smoothed indicator function based on the pressure gradient and the local cell size. Care was taken to ensure that the additional numerical smoothing in the discretization of the inviscid flux terms remains second order accurate even when there are jumps in the grid spacing. The viscous coefficient is defined by $\varepsilon = N^{-2}$, where N is the number of grid points, and the effect of the grid adaptation is to smear the shock across an increasing number of grid points as N increases.

Evaluating the combined adjoint error estimates for viscous modeling error and numerical residual error, we obtain either a sharp bound on the 2nd order base error or a 4th order functional estimate as seen in Figure 3. These results were obtained using cubic spline reconstruction, but virtually indistinguishable results were obtained using linear interpolation.

Two-dimensional Implementation

Discretization

The two-dimensional Euler equations are discretized using a 2nd order accurate cell-centered finite volume scheme with dummy cells to enforce boundary conditions. The solution is marched to a steady state using multigrid with Runge–Kutta smoothing[34,35]. Numerical dissipation scaled by the spectral radius of the flux Jacobian is based on 4th differences of the vector of conserved variables $u = (\rho, \rho q_x, \rho q_y, \rho E)^T$.

Boundary Conditions

Correct implementation of the boundary conditions is important to the order of accuracy of the functional estimates. We now briefly describe the form of the flow and adjoint boundary conditions, using boundary normals which point out of the computational domain.

For the flow equations, there is one incoming characteristic at the wall and the corresponding physical boundary conditions is

$$q_n \equiv q_x n_x + q_y n_y = 0.$$

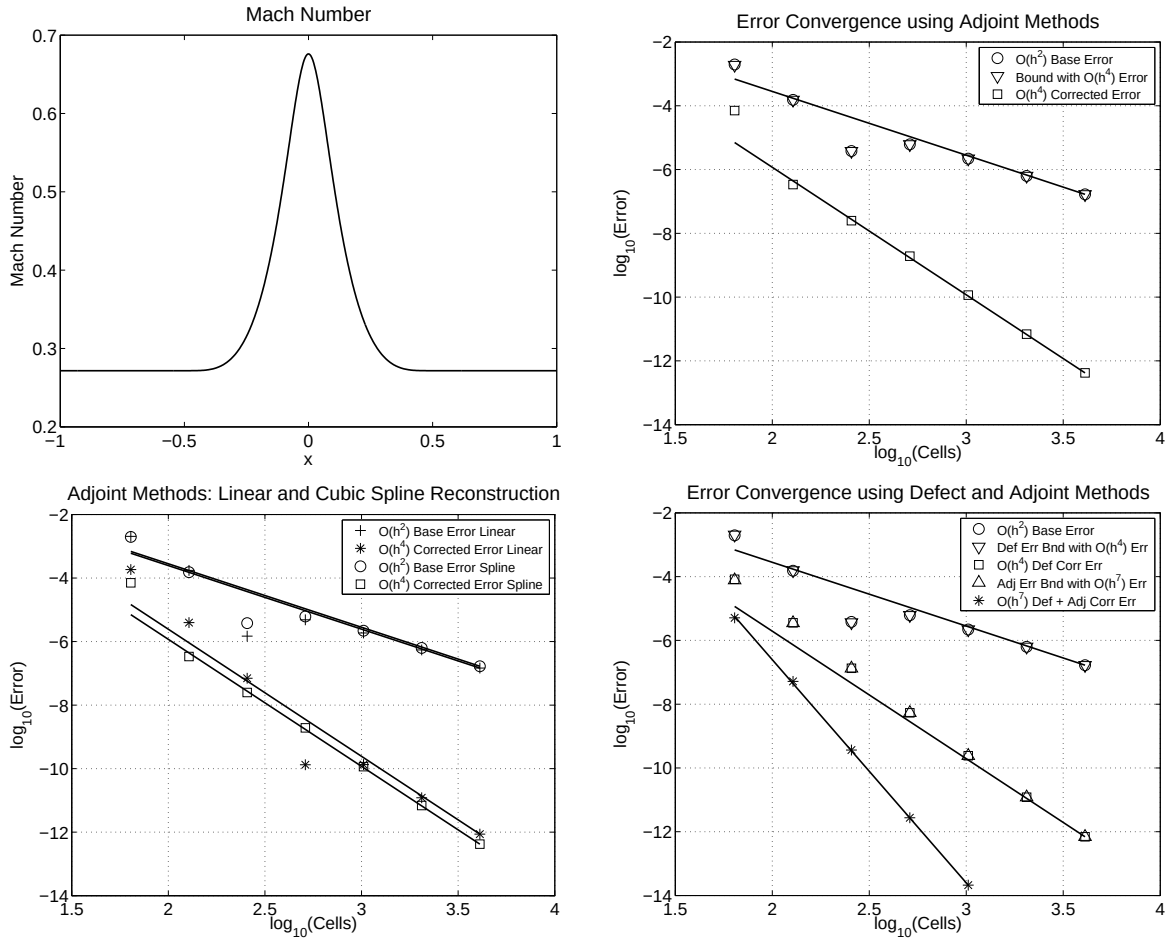

Figure 2. Subsonic quasi-1D flow. a) Mach number profile. b) Adjoint error bounding and correction using cubic spline reconstruction. c) A comparison of adjoint error correction using linear and cubic spline interpolation. d) Defect error bounding and correction supplemented by adjoint error bounding and correction. The superimposed lines have slope -2, -4 or -7 as suggested by the rate descriptions in the legends.

All conserved variables are linearly extrapolated to the dummy cells inside the wall so as to enforce zero normal velocity with second order accuracy.

At an inflow boundary, three physical boundary conditions and one numerical boundary condition must be specified. This is accomplished by using a Newton iteration to enforce

$$R \equiv \begin{pmatrix} H_\infty - \bar{H} \\ s_\infty - \bar{s} \\ q_t^{ff} - \bar{q}_t \\ \Delta p + \bar{\rho}\bar{c}\,\Delta q_n \end{pmatrix} = 0$$

at the inflow boundary, where a bar denotes an average at the boundary of the values in the adjacent interior cell and exterior dummy cell, and Δ denotes a difference in the values at these same two cells. The first three equations represent specification of the stagnation enthalpy, entropy and tangential velocity. For a modified Euler problem, q_t^{ff} is obtained from the known analytical solution. For the duct, the equation for entropy is replaced by stagnation pressure, and $q_t^{ff} = 0$. The fourth equation is a characteristic boundary condition on the outgoing characteristic.

At an outlet boundary, a Newton iteration is used to enforce one physical boundary condition and three numerical boundary conditions

$$R \equiv \begin{pmatrix} \bar{c}^2\Delta\rho - \Delta p \\ \Delta q_t \\ \Delta p + \bar{\rho}\bar{c}\,\Delta q_n) \\ p^{ff} - \bar{p} \end{pmatrix} = 0.$$

The first three equations represent characteristic boundary conditions on the three outgoing charac-

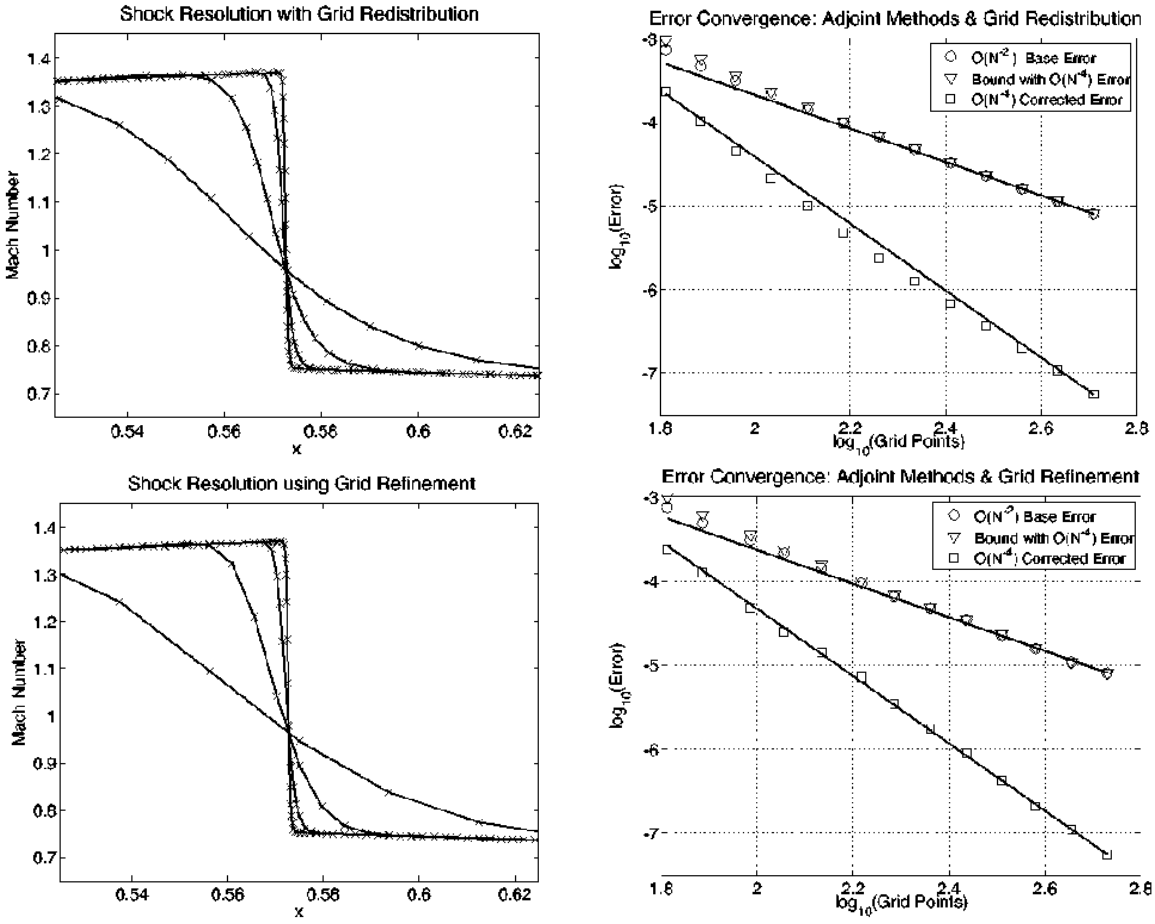

Figure 3. Shocked quasi-1D flow. Mach number distribution on a sequence of meshes with adaptive resolution of the shock provided by a) grid refinement, c) grid redistribution. Adjoint error bounding and correction using cubic spline reconstruction with b) grid refinement, d) grid redistribution. The superimposed lines have slope -2 and -4.

teristics and the fourth equation sets the exit pressure based on a far field model. For the duct, the exit pressure is uniform and for the airfoil, it is based on the known solution to the modified Euler equations.

The adjoint boundary conditions are defined so as to remove the dependence of the augmented linearized functional on perturbations to the flow variables[28,36].

For the adjoint equations, the flow of information along characteristics is reversed. At the wall, there is one outgoing flow characteristic and hence one adjoint boundary condition. The specific boundary condition depends on the choice of integral functional. If the linearized form of the nonlinear functional is $(h, \frac{\partial p}{\partial u}\tilde{u})_{\partial\Omega}$, corresponding to a weighted integral of the surface pressure perturbation, then the adjoint boundary condition has the form[28,29]

$$v_2 n_x + v_3 n_y = h,$$

which is enforced at the wall with second order accuracy.

At inlet and outlet boundary conditions, the linearized augmented functional contains an expression of the form[28,29]

$$v^T A_n \tilde{u},$$

where A_n is the flux Jacobian in the coordinate system normal to the boundary. For convenience, the boundary term may be written in the equivalent characteristic form

$$\psi^T \Lambda \tilde{\Omega}.$$

Here, the characteristic adjoint and flow variables are

$$\psi = T^T v, \quad \tilde{\Omega} = T^{-1}\tilde{u},$$

Λ is the diagonal matrix of eigenvalues of A_n and T is the matrix of right eigenvectors of A_n. This

characteristic form may be partitioned into incoming and outgoing adjoint and flow components to give

$$\psi_{\rm out}^T \Lambda_{\rm in} \tilde{\Omega}_{\rm in} + \psi_{\rm in}^T \Lambda_{\rm out} \tilde{\Omega}_{\rm out}, \qquad (9)$$

where the number of incoming flow and outgoing adjoint components is identical. Likewise, there are the same number of incoming adjoint and outgoing flow components.

Outgoing adjoint characteristic components $\psi_{\rm out}$ are linearly extrapolated to the boundary of the domain. The incoming characteristic flow perturbations $\tilde{\Omega}_{\rm in}$ are expressed in terms of the unknown outgoing perturbations $\tilde{\Omega}_{\rm out}$ by invoking the flow boundary condition $R = 0$. The effect of perturbations to incoming and outgoing characteristic variables on R is described by

$$D_{\rm in} \tilde{\Omega}_{\rm in} + D_{\rm out} \tilde{\Omega}_{\rm out} = \delta R$$

where

$$\left(D_{\rm in} | D_{\rm out} \right) = \frac{\partial R}{\partial u} T.$$

Perturbations to the incoming characteristic variables may then be expressed

$$\tilde{\Omega}_{\rm in} = -D_{\rm in}^{-1} D_{\rm out} \tilde{\Omega}_{\rm out}.$$

Using this to eliminate $\Omega_{\rm in}$, the boundary term (9) becomes

$$\left(\psi_{\rm in}^T \Lambda_{\rm out} - \psi_{\rm out}^T \Lambda_{\rm in} D_{\rm in}^{-1} D_{\rm out} \right) \tilde{\Omega}_{\rm out}.$$

Making this zero for any $\tilde{\Omega}_{\rm out}$ requires the adjoint boundary condition

$$\psi_{\rm in} = \Lambda_{\rm out}^{-1} \left(D_{\rm in}^{-1} D_{\rm out} \right)^T \Lambda_{\rm in} \, \psi_{\rm out}.$$

Reconstruction

For the two-dimensional Euler equations, the discrete solution is computed at the cell centers of a structured quadrilateral mesh. The solution is averaged to the grid nodes prior to reconstruction so that the mesh and the solution are defined at the same locations. The analytical wall and far field boundary conditions are then enforced at the mesh points prior to reconstruction. The wall boundary condition makes use of the exact wall normals to enforce flow tangency. This boundary fix makes it unnecessary to evaluate the boundary contribution to the adjoint error estimate because the leading term in the boundary residual is shifted into the interior of the domain.

The approximate solutions u_h and v_h are then formed using bi-cubic spline interpolation for each component. Not-a-knot boundary conditions are employed except in cases where one of the computational coordinates is periodic[37]. The coordinate data is also splined, so that the solutions and coordinates, u_h, v_h, x_h, y_h, are all defined parametrically as functions of the two spline coordinates ξ, η. Derivatives of each component of u_h can then be evaluated by solving

$$\begin{pmatrix} \frac{\partial u_h}{\partial \xi} \\ \frac{\partial u_h}{\partial \eta} \end{pmatrix} = \begin{pmatrix} \frac{\partial x_h}{\partial \xi} & \frac{\partial y_h}{\partial \xi} \\ \frac{\partial x_h}{\partial \eta} & \frac{\partial y_h}{\partial \eta} \end{pmatrix} \begin{pmatrix} \frac{\partial u_h}{\partial x} \\ \frac{\partial u_h}{\partial y} \end{pmatrix}.$$

The error correction integral is evaluated in (ξ, η) coordinates using 3×3 Gauss quadrature on each cell.

The boundary fix procedure is also useful for reconstructed solutions that are used to drive a defect iteration. The defect transfer operator T_h that defines the source term at each cell center is based on the average value of the source term over the computational cell evaluated using 3×3 Gauss quadrature.

Note that the residuals that drive the defect iteration are based on a discrete solution defined at the grid nodes. The process of averaging from the cell centers to the grid nodes may be interpreted as part of the overall 2nd order accurate discretization procedure. The defect iteration produces a solution at the cell centers that becomes 4th order accurate only after the discretization process is completed by again averaging to the grid nodes. This interesting property simplifies the issue of moving solution data to the nodes.

When using defect or adjoint methods alone, the approaches described above suffice to provide 4th order accuracy. However, when attempting to achieve 6th order accuracy, there are additional sources of error that must be considered. After defect correction, the present scheme defines a reconstructed flow solution that is 4th order accurate and an adjoint solution that is 2nd order with a splined geometry that is 4th order accurate. One source of remaining error is the boundary residual contribution to the adjoint correction (which is not necessary for 4th order accuracy when using the boundary fix described above). Another source of error is the evaluation of boundary integrals on the approximate geometry. There is also an error in the bulk adjoint correction term resulting from the neglect of the slivers that exist between the splined and true geometries. However, these contributions should be $O(h^6)$ since the total neglected area is $O(h^4)$ and the residual integrated over this area is $O(h^2)$. A careful investigation of each source of error is currently underway.

Modified Euler equations

2D Duct. The flow field is defined to be the exact quasi-1D flow solution[38] with a vertical velocity component that varies linearly from the upper to lower walls so as to satisfy flow tangency

$$q_y = q_x \frac{da}{dx}\frac{y}{a}.$$

Here, $a(x) = \frac{1}{2}A(x)$ is the half-height of the duct and $y = 0$ is an axis of symmetry. The constructed solution u_m is substituted into the 2D Euler operator N to obtain a source term to drive the modified Euler equations

$$f_m \equiv N(u_m).$$

Derivatives of the flow quantities may be obtained using standard differential relations between the flow quantities and the duct variation[38].

Subsonic Cylinder. The velocity field is defined to correspond to incompressible flow around a cylinder. Using standard complex potential flow methods[39], the geometry is defined by $|w| = 1$ in the complex $w = u + iv$ plane, and the velocity field is based on the complex potential

$$\Phi = q_0(w + w^{-1})$$

where q_0 is the real free stream velocity magnitude. The Cartesian velocity components q_u and q_v are obtained from

$$q_u - iq_v = \frac{d\Phi}{dw}$$

with derivatives

$$\frac{\partial q_u}{\partial u} = -\frac{\partial q_v}{\partial v} = \mathcal{R}\left\{\frac{d^2\Phi}{dw^2}\right\},$$
$$\frac{\partial q_v}{\partial u} = \frac{\partial q_u}{\partial v} = -\mathcal{I}\left\{\frac{d^2\Phi}{dw^2}\right\}.$$

Given this definition of the velocity, the pressure and density, and their derivatives, are then defined by specifying uniform stagnation enthalpy H and entropy s throughout the flow field.

Subsonic Lifting Airfoil. The velocity field over a subsonic lifting Joukowski airfoil is again specified to correspond to incompressible flow, and is obtained by constructing a complex potential using conformal mapping[39]. Starting from the unit cylinder $|w| = 1$ in the $w = u + iv$ plane, we first map to a shifted scaled cylinder in the $z = x + iy$ plane centered at

$$\gamma = \varepsilon_x - \mathrm{i}\varepsilon_y, \quad \varepsilon_x, \varepsilon_y > 0,$$

with radius $R = |1+\gamma|$. The mapping from w to z is

$$z = -\gamma + R\mathrm{e}^{\mathrm{i}\alpha}w,$$

and the inverse mapping is

$$w = R^{-1}\mathrm{e}^{-\mathrm{i}\alpha}(z + \gamma),$$

where α is the angle of attack. The cylinder in the z plane is then mapped to a Joukowski airfoil in the $c = a + ib$ plane using

$$c = \tfrac{1}{2}(z + z^{-1})$$

with inverse mapping

$$z = c + \sqrt{c^2 - 1}.$$

Care must be taken to define the branch cut for the square root to lie inside the airfoil geometry.

The trailing edge of the airfoil is at $c = 1$, which corresponds to $z = 1$ and

$$w = \mathrm{e}^{-\mathrm{i}(\alpha+\beta)}, \quad \tan\beta \equiv \frac{\varepsilon_y}{1 + \varepsilon_x}.$$

We also need the following geometry mapping derivatives:

$$\frac{\mathrm{d}z}{\mathrm{d}w} = R\mathrm{e}^{\mathrm{i}\alpha}, \quad \frac{\mathrm{d}w}{\mathrm{d}z} = R^{-1}\mathrm{e}^{-\mathrm{i}\alpha},$$

and

$$\frac{\mathrm{d}c}{\mathrm{d}z} = \tfrac{1}{2}(1 - z^{-2}), \quad \frac{\mathrm{d}z}{\mathrm{d}c} = 1 + \frac{c}{\sqrt{c^2 - 1}}.$$

The complex potential in the w-plane is

$$\Phi = q_0\left(w + w^{-1}\right) + \mathrm{i}\Gamma\log w,$$

with q_0 being real. The Cartesian velocity components, q_a and q_b, in the c-plane are then

$$q_a - \mathrm{i}q_b = \frac{\mathrm{d}\Phi}{\mathrm{d}c} = \frac{\mathrm{d}\Phi}{\mathrm{d}w}\frac{\mathrm{d}w}{\mathrm{d}z}\frac{\mathrm{d}z}{\mathrm{d}c}. \tag{10}$$

Asymptotically, as $c \to \infty$, $q_a - \mathrm{i}q_b \to 2R^{-1}\mathrm{e}^{-\mathrm{i}\alpha}q_0$, so a freestream speed q_∞ at angle of attack α requires

$$q_0 = \tfrac{1}{2}Rq_\infty.$$

There is a critical point in the Joukowski mapping at the cusped trailing edge, where $\frac{\mathrm{d}c}{\mathrm{d}z} = 0$ at $c = 1$. Examining the expression for complex velocity (10), the Kutta condition requires that $\frac{\mathrm{d}\Phi}{\mathrm{d}w} = 0$ as well. This corresponds to placing a stagnation point in the w plane at $w = \mathrm{e}^{-\mathrm{i}(\alpha+\beta)}$. The corresponding vortex strength leading to smooth flow at the trailing edge is

$$\Gamma = 2q_0\sin(\alpha + \beta).$$

The velocity expression (10) is indeterminate at the cusped trailing edge, but the velocity at this point can be found using l'Hopital's rule

$$q_a - \mathrm{i}q_b = \left(2q_0 w^{-3} - \mathrm{i}\Gamma w^{-2}\right)\left(\frac{\mathrm{d}w}{\mathrm{d}z}\right)^2,$$

with $w = \mathrm{e}^{-\mathrm{i}(\alpha+\beta)}$. The flow derivatives are obtained from

$$\frac{\mathrm{d}^2\Phi}{\mathrm{d}c^2} = \frac{\mathrm{d}^2\Phi}{\mathrm{d}w^2}\left(\frac{\mathrm{d}w}{\mathrm{d}z}\frac{\mathrm{d}z}{\mathrm{d}c}\right)^2 + \frac{\mathrm{d}\Phi}{\mathrm{d}w}\frac{\mathrm{d}w}{\mathrm{d}z}\frac{\mathrm{d}^2 z}{\mathrm{d}c^2}.$$

with

$$\frac{\partial q_a}{\partial a} = -\frac{\partial q_b}{\partial b} = \mathcal{R}\left\{\frac{\mathrm{d}^2\Phi}{\mathrm{d}c^2}\right\},$$

$$\frac{\partial q_b}{\partial a} = \frac{\partial q_b}{\partial a} = -\mathcal{I}\left\{\frac{\mathrm{d}^2\Phi}{\mathrm{d}c^2}\right\}.$$

The pressure and density are again obtained by specifying uniform stagnation enthalpy and entropy throughout the flow field.

Two-dimensional Results

Subsonic 2D duct

We now consider adjoint and defect methods for subsonic Euler flow in a smooth 2D duct. We consider the drag functional, which should be identically zero for this problem. In developing the implementation, we found it very helpful to work on a test case where the solution is known in addition to the functional value. In a subsequent section, we describe a modified Euler problem for 2D duct geometries that has a known analytical solution. For the present studies, we return to the unmodified Euler equations and rescale the geometry used for the quasi-1D test case (8) to be ten times longer. The same inlet and outlet conditions are used with the additional restriction that the flow is uniform at the inlet ($q_y = 0$). The equations are discretized using a 2nd order accuracy finite volume scheme. Reconstruction is performed using bi-cubic splining with not-a-knot boundary conditions[37]. Boundary integrals are evaluated using 3 point Gauss quadrature and bulk integrals are evaluated using 3×3 Gauss quadrature. Figure 4a depicts a sample computational mesh, computed pressure contours, and residual contours obtained by substituting the reconstructed solution into the first component of the Euler equations.

The baseline drag estimate are $O(h^3)$ for this problem, as illustrated in Figure 4b. Adjoint methods provide either a sharp bound that is in error by $O(h^5)$, or else an $O(h^5)$ functional estimate. The numerical discretization provides $O(h^2)$ primal and dual solutions and cubic spline reconstruction provides a residual with the same order of accuracy. Hence we expect at least 2nd order functional accuracy before correction and 4th order accuracy after correction. In the present setting, we observe an additional order of accuracy in each case. These results are reproducible on ducts with different throat constrictions or asymmetric shape changes.

Figure 4c illustrates that linear reconstruction provides nearly identical performance. Unlike in the quasi-1D case, a theoretical justification for this behavior is not currently available. We are not yet convinced of the generality of this result, as the performance of linear interpolation does not hold up on the airfoil test case to be discussed later. Nonetheless, linear reconstruction is very attractive from a practical viewpoint so it merits consideration until definitive conclusions are reached regarding its viability.

A combination of defect and adjoint methods are presented for this 2D duct flow in Figure 4d. Defect methods provide an error estimate that is used either to provide a sharp bound on the 2nd order baseline error or subtracted to obtain a 4th order functional estimate. Adjoint methods then provide a bound on the 4th order defect estimate or else produce a 5th order functional estimate. Note that the functional accuracy is improved by roughly an order of magnitude relative to the 5th order functional estimates obtained in Figure 4b. In theory, the primal solution after defect correction should be $O(h^4)$ and the adjoint residual should be $O(h^2)$ so we expect $O(h^6)$ functional accuracy using the combined approach. Further work is required to investigate the remaining sources of error that prevent 6th order functional convergence. A fundamental difficulty is that the reconstructed solution is defined on a splined geometry that is only 4th order accurate.

Subsonic airfoil

Our final test case examines the drag for lifting flow over a Joukowski airfoil with free stream Mach number $M_\infty = 0.5$ and angle of attack $\alpha = 3^o$. For this geometry, we construct a modified Euler problem with a known analytical solution. Constant entropy and stagnation enthalpy conditions are combined with a velocity field derived from the potential flow solution for the same geometry. The computational domain is truncated at approximately 27 chords, where the far field boundary conditions are based on the exact solution to the modified Euler problem. The exact drag is non-zero for the modified solution owing to

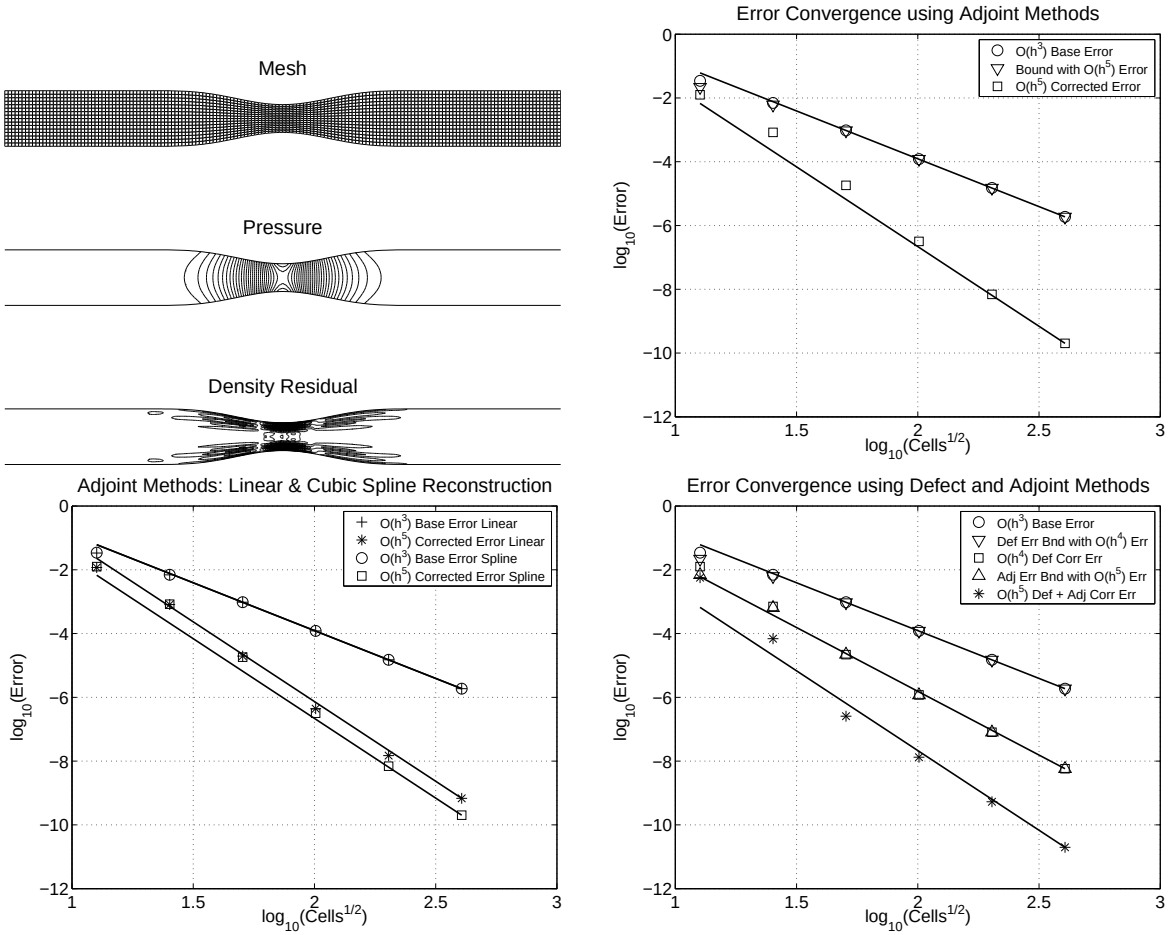

Figure 4. Subsonic flow in a duct. a) Computational mesh, computed pressure contours and reconstructed density residual. b) Adjoint error bounding and correction using cubic spline reconstruction. c) A comparison of adjoint error correction using linear and cubic spline interpolation. d) Defect error bounding and correction supplemented by adjoint error bounding and correction. The superimposed lines have slope -3, -4 or -5 as suggested by the rate descriptions in the legends.

the effects of the small forcing terms in the modified equation. The reconstruction scheme uses periodic cubic splines around the airfoil including on the wall boundary.

A sample computational mesh and corresponding pressure contours are depicted in Figures 5a and 5b. This problem is more challenging than the smooth 2D duct, since it contains a geometric singularity at the cusped trailing edge. In Figure 5c, we observe a base error in the drag that is $O(h^{2.5})$. Using adjoint error bounding we obtain an asymptotically sharp bound. Using adjoint error correction, we obtain 4th order accuracy in the functional estimate.

Conclusions

We have described adjoint and defect methods for obtaining sharp estimates of the error in integral functionals of PDE solutions. This approach has been demonstrated for the drag on a lifting airfoil in subsonic flow. Using 2nd order discretizations for the flow and adjoint systems and cubic spline solution reconstruction, we obtain either an asymptotically sharp bound on the error in the functional, or else a corrected functional estimate with 4th order accuracy. Adjoint error estimation methods have also been extended to treat shocked flows, using a two step correction process to account for modeling and discretization errors. Again, 4th order error estimates are obtained.

A modified equation approach is employed to provide test cases on interesting geometries with known

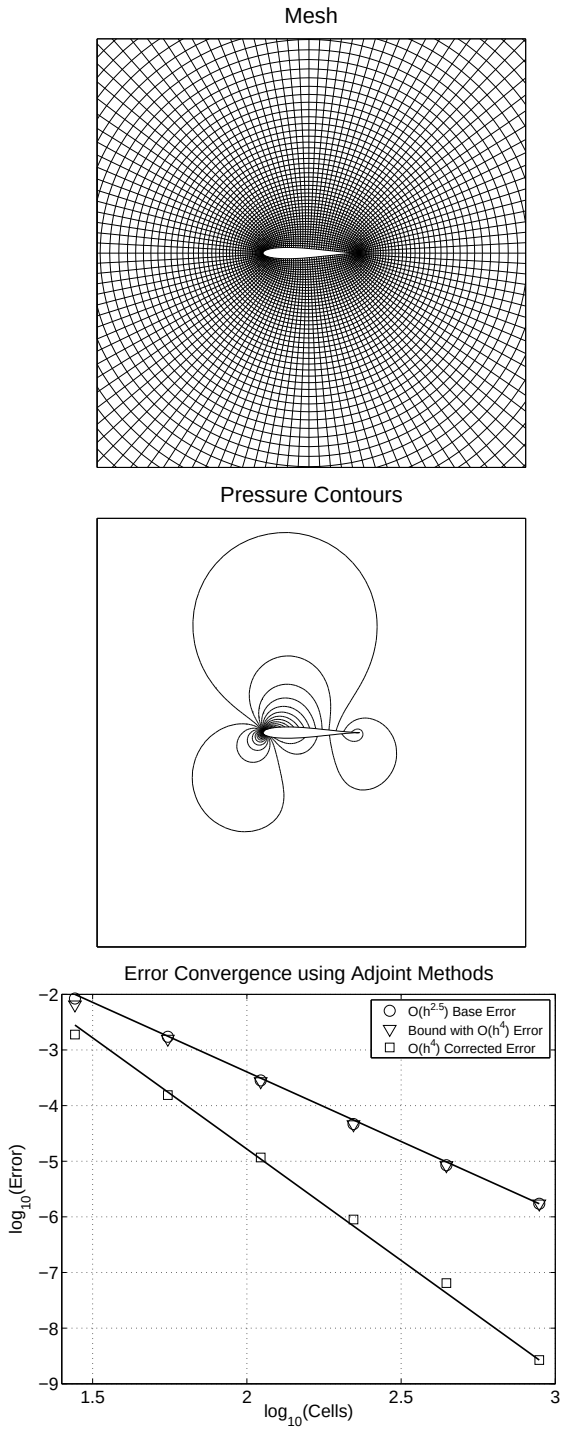

Figure 5. Subsonic flow over a lifting airfoil. a) Computational mesh, b) Computed pressure contours, c) Adjoint error bounding and correction for the error in the drag. The superimposed lines have slopes -2.5 and -4.

exact solutions. At truncated computational boundaries, the solution to the modified equation may be used to provide an exact far field model. The issue of far field model accuracy is conceptually distinct from the sources of error treated in this paper. Further studies are required to determine the impact of approximate far field models on the performance of the methods presented here. It may be interesting to consider adjoint approaches for computing the sensitivities of functional estimates to errors in the far field model. The difficulty is that some means of assessing the error in the far field model would be required to obtain a bound or perform a correction.

The present bounding and correction methods can be extended to unstructured computational meshes by changing to an unstructured reconstruction scheme[18]. A discrete version of this approach has been employed successfully on unstructured meshes[6,7], where the error estimates may be used to drive an adaptive meshing algorithm. Individual cell or element error contributions may be used to drive adaptive error control methods by "localizing" the error contribution via the triangle inequality[21]. Localization introduces a safety margin by reducing the sharpness of the bound (to the degree that it eliminates cancellation effects between elements with errors of opposite sign).

The combined use of adjoint and defect methods to attempt 6th order error estimates using 2nd order numerics and 4th order reconstruction is currently underway. These same ingredients have been used successfully for smooth quasi-1D Euler flow, even when the exact geometry is replaced by a splined representation.

Acknowledgments

This work was funded by NASA/Ames Cooperative Agreement No. NCC 2-5431.

References

1. P. Monk and E. Süli. The adaptive computation of far field patterns by a posteriori error estimates of linear functionals. *SIAM J. Numer. Anal.*, 36(1):251–274, 1998.

2. M.B. Giles and N.A. Pierce. Improved lift and drag estimates using adjoint Euler equations. In *14th AIAA Computational Fluid Dynamics Conference*, 1999. AIAA Paper 99-3293.

3. N.A. Pierce and M.B. Giles. Adjoint recovery of superconvergent funtionals from PDE approximations. *SIAM Review*, 42(2):247–264, 2000.

4. M.B. Giles and N.A. Pierce. Adjoint error correction for integral outputs. In *Lecture Notes in Computational Science & Engineering: Error Estimation and Adaptive Discretization Methods in Computational Fluid Dynamics*, volume 25. Springer, 2002.

5. M.B. Giles. Defect and adjoint error correction. In N. Satofuka, editor, *Computational Fluid Dynamics 2000*. Springer, 2001.

6. D. Venditti and D. Darmofal. Grid adaptation for functional outputs: application to two-dimensional inviscid flows. *J. Comput. Phys.*, 176:40–69, 2002.

7. D. Darmofal and D. Venditti. Anisotropic grid adaptation for functional outputs: application to two-dimensional viscous flows. *J. Comput. Phys.*, 187:22–46, 2003.

8. I. Babuška and A. Miller. The post-processing approach in the finite element method – Part 1: calculation of displacements, stresses and other higher derivatives of the displacements. *Intern. J. Numer. Methods Engrg.*, 20:1085–1109, 1984.

9. I. Babuška and A. Miller. The post-processing approach in the finite element method – part 2: the calculation of stress intensity factors. *Intern. J. Numer. Methods Engrg.*, 20:1111–1129, 1984.

10. J.W. Barrett and C.M. Elliott. Total flux estimates for a finite-element approximation of elliptic equations. *IMA J. Numer. Anal.*, 7:129–148, 1987.

11. C. Johnson, R. Rannacher, and M. Boman. Numerics and hydrodynamic stability – toward error control in computational fluid dynamics. *SIAM J. Numer. Anal.*, 32(4):1058–1079, 1995.

12. M. Paraschivoiu, J. Peraire, and A. Patera. A posteriori finite element bounds for linear-functional outputs of elliptic partial differential equations. *Comput. Methods Appl. Mech. Engrg.*, 150(1-4):289–312, 1997.

13. J. Peraire and A.T. Patera. Bounds for linear-functional outputs of coercive partial differential equations: local indicators and adaptive refinement. In P. Ladeveze and J.T. Oden, editors, *New Advances in Adaptive Computational Methods in Mechanics*. Elsevier, 1997.

14. J.T. Oden and S. Prudhomme. New approaches to error estimation and adaptivity for the Stokes and Oseen equations. *Internat. J. Numer. Methods Fluids*, 31(1):3–15, 1999.

15. P. Houston, R. Rannacher, and E. Süli. A posteriori error analysis for stabilised finite element approximations of transport problems. *Comput. Methods Appl. Mech. Engrg.*, 190(11-12):1483–1508, 2000.

16. R. Rannacher. Adaptive Galerkin finite element methods for partial differential equations. *J. Comput. Appl. Math.*, 1-2:205–233, 2000.

17. R. Becker and R. Rannacher. An optimal control approach to error control and mesh adaptation. In A. Iserles, editor, *Acta Numerica 2001*. Cambridge University Press, 2001.

18. M.B. Giles and E. Süli. Adjoints methods for PDEs: *a posteriori* error analysis and postprocessing by duality. In A. Iserles, editor, *Acta Numerica 2002*, pages 145–236. Cambridge University Press, 2002.

19. A.T. Patera and J. Peraire. A general Lagrangian formulation for the computation of *a posteriori* finite element bounds. In *Adaptive Finite Element Approximation of Hyperbolic Problems*, volume 25. Springer, 2002.

20. S. Prudhomme and J.T. Oden. Computable error estimators and adaptive techniques for fluid flow problems. In *Adaptive Finite Element Approximation of Hyperbolic Problems*, volume 25. Springer, 2002.

21. E. Süli and P. Houston. Adjoint error correction for integral outputs. In *Adaptive Finite Element Approximation of Hyperbolic Problems*, volume 25. Springer, 2002.

22. M.B. Giles and N.A. Pierce. Analytic adjoint solutions for the quasi-one-dimensional Euler equations. *J. Fluid Mech.*, 426:327–345, 2001.

23. M.B. Giles and N.A. Pierce. On the properties of solutions of the adjoint Euler equations. In M. Baines, editor, *Numerical Methods for Fluid Dynamics VI*. ICFD, 1998.

24. S. Ulbrich. A sensitivity and adjoint calculus for discontinuous solutions of hyperbolic conservation laws with source terms. *SIAM J. Control and Optim.*, 41(3):740–797, 2002.

25. S. Ulbrich. Adjoint-based derivative computations for the optimal control of discontinuous solutions of hyperbolic conservation laws. *Systems & Control Letters*, 48(3-4):313–328, 2003.

26. M.B. Giles. Discrete adjoint approximations with shocks. In T. Hou and E. Tadmor, editors, *Proceedings of Ninth International Conference on Hyperbolic Problems*. Springer-Verlag, 2003.

27. M.B. Giles and N.A. Pierce. Analysis of adjoint error correction for superconvergent functional estimates. *SIAM J. Numer. Anal.*, submitted. Oxford University Computing Laboratory Report NA 01/14, 2001.

28. A. Jameson. Optimum aerodynamic design using control theory. *Comput. Fluid Dynam. Rev.*, 3:495–528, 1995.

29. M.B. Giles and N.A. Pierce. Adjoint equations in CFD: duality, boundary conditions and solution behavior. In *13th Computational Fluid Dynamics Conference, Snowmass, CO*, 1997. AIAA Paper 97-1850.

30. A. Jameson, N.A. Pierce, and L. Martinelli. Optimum aerodynamic design using the Navier-Stokes equations. *Theor. Comput. Fluid Dyn.*, 10:213–237, 1998.

31. C.M. Bender and S.A. Orszag. *Advanced Mathematical Methods for Scientists and Engineers*. McGraw-Hill Inc, 1978.

32. J. Kevorkian and J.D. Cole. *Perturbation Methods in Applied Mathetics*. Number 34 in Applied Math Series. Springer-Verlag, 1981.

33. G. Dahlquist and A. Björck. *Numerical Methods*. Prentice–Hall, 1974.

34. A. Jameson, W. Schmidt, and E. Turkel. Numerical solution of the Euler equations by finite volume methods using Runge-Kutta time stepping schemes. AIAA Paper 81-1259, 1981.

35. A. Jameson. Solution of the Euler equations by a multigrid method. *Appl. Math. Comput.*, 13:327–356, 1983.

36. A. Jameson. Aerodynamic design via control theory. *J. Sci. Comput.*, 3:233–260, 1988.

37. C. de Boor. *A Practical Guide to Splines*. Springer, 2001.

38. H.W. Liepmann and A. Roshko. *Elements of gas dynamics*. Wiley, 1957.

39. G.K. Batchelor. *An Introduction to Fluid Dynamics*. Cambridge University Press, 1967.